


Influence of the nuclear symmetry energy slope on observables of compact stars with Δ -admixed hypernuclear matter

Vivek Baruah Thapa* and Monika Sinha†
Indian Institute of Technology Jodhpur, Jodhpur 342037, India

 (Received 14 September 2021; accepted 23 December 2021; published 4 January 2022)

In this work, we study the effects of the nuclear symmetry energy slope on the neutron star dense matter equation of state and its impact on neutron star observables (mass-radius, tidal response). We construct the equation of state within the framework of covariant density functional theory implementing coupling schemes of nonlinear and density-dependent models with viability of heavier non-nucleonic degrees of freedom. The slope of the symmetry energy parameter (L_{sym}) is adjusted following the density dependence of isovector meson coupling to baryons. We find that smaller values of L_{sym} at saturation favor early appearance of Δ resonances in comparison to hyperons, leading to latter's threshold at higher matter densities. We also investigate the dependence of L_{sym} on tidal deformability and the compactness parameter of a $1.4M_{\odot}$ neutron star for different equations of state and observe similar converging behavior for larger L_{sym} values.

DOI: [10.1103/PhysRevC.105.015802](https://doi.org/10.1103/PhysRevC.105.015802)

I. INTRODUCTION

In stellar evolution, when nuclear fusion stops and the electron degeneracy pressure cannot prevent gravitational collapse, electrons happen to combine with protons and produce neutron-rich nuclei. Eventually neutrons drip out of the nuclei, and the matter becomes mainly composed of neutrons with some admixture of protons and electrons. This remnant of stellar evolution is called a neutron star (NS). Thus, after the type-II supernova explosion the stellar remnant forms a highly dense NS. Naturally, the matter density inside the NS varies from subnuclear density near the surface to supranuclear density towards the center. Matter is composed of ions and electrons near the surface, i.e., in the outer crust region, and in the inner crust region neutron-rich nuclei and some free neutrons appear. Then, in the core, matter is completely made of free neutrons with comparatively fewer protons and electrons. With the increase of density towards the center of the star, exotic components of matter, viz., hyperons, heavier non-strange baryons, Boson condensates, and even deconfined quarks may appear, while near the surface where density is comparatively low, up to ≈ 2 times nuclear saturation density (n_0), the matter is composed of only nucleons [1,2]. Hence, the interior of NS is a good domain to study dense nuclear matter in bulk with and without exotic degrees of freedom. In general, we have good knowledge about finite nuclei at n_0 . Hence, the theoretical idea of uniform symmetric nuclear matter in bulk even at varied densities above n_0 is just the extrapolation and idealization of finite nuclei knowledge. On the other hand, the observational test of bulk matter properties

in varied density above n_0 can only be obtained from astrophysical observations of compact NSs.

One important ingredient for energy density of nucleons inside nuclear matter is the symmetry energy (E_{sym}). Consequently, nuclear symmetry energy and its density dependence play a salient role in comprehending dense matter behavior [3,4]. In case of finite nuclei, the contribution of symmetry energy to the mass of the nuclei is small compared to other terms in the semiempirical mass formula. Hence, the experimental information regarding E_{sym} is not very sound even at n_0 . As mentioned earlier, from the astrophysical properties of NSs the nuclear matter properties at varied density can be determined. The nuclear symmetry energy and its variation with density affect substantially the composition and matter pressure, which consequently affects the NS properties, especially the radius [5,6]. Although from nuclear data we have very little knowledge of E_{sym} , a good comprehensive idea of the same can now be drawn from the recent radius measurement of certain NS candidates, PSR J0030 + 0451 [7–9] and PSR J0740 + 6620 [10,11] from the NICER (Neutron star Interior Composition Explorer) space mission. The detection of gravitational wave (GW) emissions from binary NS mergers (GW170817 [12–14] and GW190425 [15]) by the LIGO-Virgo Collaboration (LVC) marked an appreciable breakthrough in the domain of multimessenger astronomy. The GW observations set a bound on the mutual tidal deformability ($\tilde{\Lambda}$), which also depends on the matter properties linked with E_{sym} .

Not only that, a comprehensive idea regarding symmetry energy behavior can be gathered via studying its effects on other NS properties such as maximum mass, compactness, and tidal deformability. The observational estimations of certain parameters, viz., maximum mass and radius of compact objects, impose vital constraints on narrowing down to a unique dense matter equation of state (EOS). For instance,

*thapa.1@iitj.ac.in

†ms@iitj.ac.in

with the observations of massive compact stars ($M \geq 2M_\odot$) such as PSR J1614–2230 ($1.908 \pm 0.016 M_\odot$) [16,17], PSR J0348+0432 ($2.01 \pm 0.04 M_\odot$) [18], and PSR J0740+6620 ($2.08^{+0.07}_{-0.07} M_\odot$ with 68.3% credibility [19]), the soft EOSs tend to be invalid. The mass-radius measurements of PSR J0030+0451 [7–9] and PSR J0740+6620 [10,11] from the NICER space mission provide a significant constraint on the dense matter EOS. The latest NICER mass-radius measurement (PSR J0740+6620) suggests repulsive matter behavior at higher density regimes. Joint analysis of data from NICER observations for PSR J0030+0451 and the GW170817 event provides bounds on NS properties, viz., tidal deformability ($\Lambda_{1.4}$) and radius ($R_{1.4}$) for a $1.4M_\odot$ star [20].

Many recent studies have been done to constrain the values of E_{sym} at n_0 and its slope (L_{sym}) at n_0 based on data from various astrophysical observations as well as terrestrial experiments [21–23]. Very recently an improved value of neutron skin thickness of ^{208}Pb was reported in the Lead Radius EXperiment-II (PREX-2) to be $R_{\text{skin}} = R_n - R_p = (0.283 \pm 0.071)$ fm [24]. This evaluates the corresponding symmetry energy and its slope to be $E_{\text{sym}} = (38.1 \pm 4.7)$ MeV and $L_{\text{sym}} = (106 \pm 37)$ MeV respectively at n_0 with correlation coefficient as 0.978 [25]. These updated values of isospin asymmetry parameters are larger than the ones [$28.5 \leq E_{\text{sym}}(n_0) \leq 34.9$ MeV, $30.6 \leq L_{\text{sym}}(n_0) \leq 86.8$ MeV] previously reported in Ref. [26], obtained by comparison of experimental data from finite nuclei and heavy-ion collisions with different microscopic model calculations. In this work, we explore the influence of nuclear symmetry energy on the dense matter EOS, and consequently on NS properties. As a consequence, we attempt to constrain the E_{sym} and L_{sym} using the observational features of NSs. To do so, we consider a covariant density functional (CDF) model implementing the density dependence of isovector-vector coupling as introduced in Ref. [27] and incorporating nonlinear GM1 [28] and density-dependent DD-MEX [29] coupling parametrizations. In the CDF scheme, the coupling constants are chosen in such a way that the model can reproduce the experimental quantities known at n_0 . Thus the observational properties of NSs which depend on the EOS parameters, i.e., coupling constants, will determine E_{sym} and L_{sym} . In several previous studies the symmetry energy effects on dense matter have been considered with the matter composition being purely nucleonic [30–32]. However, due to increasing Fermi energy of nucleons in the interior of the NS, the appearance of additional degrees of freedom such as hyperons [28,33–41], Δ resonances [42–52], and meson (π , \bar{K} , ρ) condensations [53–60] are inevitable or energetically favorable for massive stars, as recently observed [16–19]. Moreover, the appearance of these exotic matter softens the EOS, reducing the maximum mass of the stars, which is contrary to the observations. Hence, the choice of EOS parametrization is limited by the observational constraints of massive stars. For that we have chosen two EOS parametrizations within the CDF model, viz., GM1 with the nonlinear model and DD-MEX with a density-dependent coupling constant, which satisfy the observational constraints of massive stars. This work will therefore explore the novel aspects of density-dependent isovector coupling on the dense matter EOS with the onset of heavier strange and nonstrange

degrees of freedom and study the symmetry energy slope effects on NS properties.

The paper is organized as follows. In Sec. II, we briefly describe the CDF model formalism, its extension to additional heavier degrees of freedom, and coupling parameters for constructing the EOS. The effects of nuclear symmetry energy on dense matter are shown and discussed in Sec. III. Section IV provides the summary and conclusions of this work.

Conventions. We implement the natural units $G = \hbar = c = 1$ throughout the work.

II. FORMALISM

A. CDF Model

This section briefly describes the CDF model implemented in this work to construct the dense matter EOS. The dense matter composition considered in this work is the entire baryon octet ($N \equiv n, p; Y \equiv \Lambda^0, \Sigma^{\pm,0}, \Xi^{-,0}$) and Δ resonances ($\Delta \equiv \Delta^+, \Delta^{++}, \Delta^0, \Delta^-$) along with leptons ($l \equiv e^-, \mu^-$). In order to mediate the effective interactions between the baryons, isoscalar-scalar σ , isoscalar-vector ω , and isovector-vector ρ mesons are considered. An additional hidden strangeness isoscalar-vector ϕ meson is also brought into consideration to describe the hyperon-hyperon repulsive interactions. The total Lagrangian density is given by [1,47]

$$\begin{aligned} \mathcal{L} = & \sum_{b \equiv N, Y} \bar{\psi}_b (i\gamma_\mu D_{(b)}^\mu - m_b^*) \psi_b + \sum_l \bar{\psi}_l (i\gamma_\mu \partial^\mu - m_l) \psi_l \\ & + \sum_\Delta \bar{\psi}_\Delta (i\gamma_\mu D_{(\Delta)}^\mu - m_\Delta^*) \psi_\Delta + \frac{1}{2} (\partial_\mu \sigma \partial^\mu \sigma - m_\sigma^2 \sigma^2) \\ & - \frac{1}{4} \omega_{\mu\nu} \omega^{\mu\nu} + \frac{1}{2} m_\omega^2 \omega_\mu \omega^\mu - \frac{1}{4} \rho_{\mu\nu} \cdot \rho^{\mu\nu} + \frac{1}{2} m_\rho^2 \rho_\mu \cdot \rho^\mu \\ & - \frac{1}{4} \phi_{\mu\nu} \phi^{\mu\nu} + \frac{1}{2} m_\phi^2 \phi_\mu \phi^\mu - U(\sigma), \end{aligned} \quad (1)$$

where the baryon octet, lepton Dirac, and Δ baryon Schwinger-Rarita fields are represented by ψ_b , ψ_l , and ψ_Δ respectively. The covariant derivative is given by $D_{\mu(j)} = \partial_\mu + ig_{\omega j} \omega_\mu + ig_{\rho j} \boldsymbol{\tau}_{j3} \cdot \boldsymbol{\rho}_\mu + ig_{\phi j} \phi_\mu$ with j denoting the baryon particle spectrum. The isospin projection of the third component of isovector-vector meson field is represented by $\boldsymbol{\tau}_{j3}$. The scalar self-interaction term, which is present only in the nonlinear model, introduced to account for the incompressibility [1], is given by

$$U(\sigma) = \frac{1}{3} g_2 \sigma^3 + \frac{1}{4} g_3 \sigma^4, \quad (2)$$

where g_2, g_3 are the coefficients of self-interactions. $\omega_{\mu\nu}$, $\rho_{\mu\nu}$, and $\phi_{\mu\nu}$ are the antisymmetric field tensors corresponding to vector meson fields and are given by

$$\begin{aligned} \omega_{\mu\nu} &= \partial_\mu \omega_\nu - \partial_\nu \omega_\mu, \\ \rho_{\mu\nu} &= \partial_\mu \boldsymbol{\rho}_\nu - \partial_\nu \boldsymbol{\rho}_\mu, \\ \phi_{\mu\nu} &= \partial_\mu \phi_\nu - \partial_\nu \phi_\mu. \end{aligned} \quad (3)$$

The Dirac and Schwinger-Rarita effective masses are respectively given by

$$m_b^* = m_b - g_{\sigma b} \sigma, \quad m_\Delta^* = m_\Delta - g_{\sigma \Delta} \sigma \quad (4)$$

with m_b, m_Δ representing the bare masses of the baryon-octet and Δ -quartet particle spectrum respectively. In mean-field approximation, the nonvanishing meson fields obtained by solving the Euler-Lagrange equations are given by

$$\begin{aligned}\sigma &= -\frac{1}{m_\sigma^2} \frac{\partial U}{\partial \sigma} + \sum_b \frac{1}{m_\sigma^2} g_{\sigma b} n_b^s + \sum_\Delta \frac{1}{m_\sigma^2} g_{\sigma \Delta} n_\Delta^s, \\ \omega_0 &= \sum_b \frac{1}{m_\omega^2} g_{\omega b} n_b + \sum_\Delta \frac{1}{m_\omega^2} g_{\omega \Delta} n_\Delta, \\ \rho_{03} &= \sum_b \frac{1}{m_\rho^2} g_{\rho b} \tau_{b3} n_b + \sum_\Delta \frac{1}{m_\rho^2} g_{\rho \Delta} \tau_{\Delta 3} n_\Delta, \\ \phi_0 &= \sum_Y \frac{1}{m_\phi^2} g_{\phi Y} n_Y.\end{aligned}\quad (5)$$

The scalar and vector (number) densities of the constituent particle spectrum are given by $n^s = \langle \bar{\psi} \psi \rangle$ and $n = \langle \bar{\psi} \gamma^0 \psi \rangle$ respectively. The chemical equilibrium conditions between species in the particle spectrum when strangeness is not conserved is given by [42,56]

$$\mu_j = \mu_n - q_j \mu_e, \quad (6)$$

where q_j is the charge of j th baryon, and μ_e, μ_n denote the chemical potentials of the electron and neutron respectively. The chemical potential of the j th baryon is defined as

$$\mu_j = \sqrt{p_{F_j}^2 + m_j^{*2}} + \Sigma^0 + \Sigma^r, \quad (7)$$

with $\Sigma^0 = g_{\omega j} \omega_0 + g_{\phi j} \phi_0 + g_{\rho j} \tau_{j3} \rho_{03}$, and the rearrangement term necessary to maintain thermodynamic consistency is given by

$$\begin{aligned}\Sigma^r &= \sum_b \left[\frac{\partial g_{\omega b}}{\partial n} \omega_0 n_b - \frac{\partial g_{\sigma b}}{\partial n} \sigma n_b^s + \frac{\partial g_{\rho b}}{\partial n} \rho_{03} \tau_{b3} n_b \right. \\ &\quad \left. + \frac{\partial g_{\phi b}}{\partial n} \phi_0 n_b \right] + \sum_\Delta (\psi_b \rightarrow \psi_\Delta^v).\end{aligned}\quad (8)$$

In the case of the nonlinear coupling model for this present work, only the isovector ρ -meson coupling contributes to the rearrangement term.

The dense matter EOS is calculated self-consistently, taking into account two additional constraints, viz., charge neutrality and global baryon number conservation, respectively given by

$$\begin{aligned}\sum_b q_b n_b + \sum_\Delta q_\Delta n_\Delta - n_e - n_\mu &= 0, \\ \sum_b n_b + \sum_\Delta n_\Delta &= n.\end{aligned}\quad (9)$$

The total energy density is given by

$$\begin{aligned}\varepsilon &= \frac{1}{2} m_\sigma^2 \sigma^2 + \frac{1}{2} m_\omega^2 \omega_0^2 + \frac{1}{2} m_\rho^2 \rho_{03}^2 + \frac{1}{2} m_\phi^2 \phi_0^2 \\ &\quad + \sum_{j=b,\Delta} \frac{2J_j + 1}{2\pi^2} \left[p_{F_j} E_{F_j}^3 - \frac{m_j^{*2}}{8} \left\{ p_{F_j} E_{F_j} \right\} \right]\end{aligned}$$

$$\begin{aligned}&+ m_j^{*2} \ln \left(\frac{p_{F_j} + E_{F_j}}{m_j^*} \right) \Bigg] + \frac{1}{\pi^2} \sum_l \left[p_{F_l} E_{F_l}^3 \right. \\ &\quad \left. - \frac{m_l^2}{8} \left\{ p_{F_l} E_{F_l} + m_l^2 \ln \left(\frac{p_{F_l} + E_{F_l}}{m_l} \right) \right\} \right].\end{aligned}\quad (10)$$

The matter pressure is then evaluated following the Gibbs-Duhem relation defined as

$$P = \sum_{j=b,\Delta} \mu_j n_j + \sum_l \mu_l n_l - \varepsilon. \quad (11)$$

B. NS structure and properties

The NS properties (mass-radius) are deduced from the Tolman-Oppenheimer-Volkoff (TOV) equations for nonrotating, spherically symmetric NS configurations corresponding to constructed EOSs which are given by [1]

$$\begin{aligned}\frac{dP(r)}{dr} &= -\frac{[\varepsilon(r) + P(r)][M(r) + 4\pi r^3 P(r)]}{r^2 [1 - 2M(r)/r]}, \\ \frac{dM(r)}{dr} &= 4\pi r^2 \varepsilon(r),\end{aligned}\quad (12)$$

where $M(r)$ is the gravitational mass enclosed within radius r . Solutions of TOV equations are obtained on applying the boundary conditions, $P(R) = M(0) = 0$.

The tidal response of compact stars to an external gravitational field is quantified in terms of dimensionless tidal deformability, defined as [61]

$$\Lambda = \frac{2}{3} k_2 \left(\frac{M}{R} \right)^{-5}, \quad (13)$$

where k_2 is the tidal Love number, defined as

$$\begin{aligned}k_2 &= \frac{8C^5}{5} (1 - 2C^2) [2 + 2C(y - 1) - y] \cdot \\ &\quad \times \{ 2C[6 - 3y + 3C(5y - 8)] + 4C^3[13 - 11y \\ &\quad + C(3y - 2) + 2C^2(1 + y)] + 3(1 - 2C^2) \cdot \\ &\quad \times [2 - y + 2C(y - 1)] \ln(1 - 2C) \}^{-1}\end{aligned}\quad (14)$$

and obtained by solving the differential equation [62],

$$r \frac{dy(r)}{dr} + y(r)^2 + y(r)F(r) + r^2 Q(r) = 0, \quad (15)$$

with boundary condition $y(0) = 2$ where the functions are defined as

$$F(r) = \frac{r - 4\pi r^3 [\varepsilon(r) - P(r)]}{r - 2M(r)}, \quad (16)$$

$$\begin{aligned}Q(r) &= \frac{4\pi r [5\varepsilon(r) + 9P(r) + \frac{\varepsilon(r)+P(r)}{\partial P(r)/\partial \varepsilon(r)}]}{r - 2M(r)} \\ &\quad - 4 \left[\frac{M(r) + 4\pi r^3 P(r)}{r^2 [1 - 2M(r)/r]} \right].\end{aligned}\quad (17)$$

In binary NS mergers, the tidal response is encoded in the combined dimensionless tidal deformability parameter, given by [63]

$$\tilde{\Lambda} = \frac{16}{13} \frac{(M_1 + 12M_2)M_1^4 \Lambda_1 + (M_2 + 12M_1)M_2^4 \Lambda_2}{(M_1 + M_2)^5}. \quad (18)$$

TABLE I. Top: Parameter values of CDF coupling models considered in this work. Bottom: Coefficient values corresponding to Eqs. (19), (21) in the DD-MEX coupling model.

Coupling model	$g_{\sigma N}$	$g_{\omega N}$	$g_{\rho N}$	g_2 (fm ⁻¹)	g_3	m_σ (MeV)	m_ω (MeV)	m_ρ (MeV)	m_ϕ (MeV)
GM1	9.5708	10.5964	8.1957	12.2817	-8.9780	550	783	770	1019.45
DD-MEX	10.7067	13.3388	7.2380			547.3327	783	763	1019.45
Meson (i)	a_i		b_i		c_i		d_i		
σ	1.3970		1.3350		2.0671		0.4016		
ω	1.3926		1.0191		1.6060		0.4556		
ρ	0.6202								

where Λ_1, Λ_2 are the dimensionless tidal deformabilities corresponding to stars with masses M_1 and M_2 respectively.

C. Coupling parameters

As mentioned earlier in Sec. I, in the present work, we implement GM1 parametrization [28] with density dependence of the isovector-vector ρ meson for meson-baryon couplings [27] and DD-MEX parametrization [29]. In case of GM1 parametrization, the density-dependent coupling constant for the isovector ρ meson is given by

$$g_{\rho N}(n) = g_{\rho N}(n_0)e^{-a_\rho(x-1)}, \quad (19)$$

where $x = n/n_0$, while the coupling constants for σ and ω mesons are considered to be density independent.

In the case of the density-dependent model, the isoscalar meson-nucleon couplings are defined as

$$g_{iN}(n) = g_{iN}(n_0)f_i(x) \quad \text{for } i = \sigma, \omega, \quad (20)$$

where the function is given by

$$f_i(x) = a_i \frac{1 + b_i(x + d_i)^2}{1 + c_i(x + d_i)^2} \quad (21)$$

and the density dependence of isovector-vector ρ -meson coupling is given by Eq. (19). Table I provides the parameter values of GM1 and DD-MEX coupling parametrizations in the nucleonic sector. In the standard GM1 parametrization $g_{\rho N}$ is density independent, and for the standard DD-MEX parametrization the coefficient a_ρ is given in Table I. For variation in L_{sym} , it is evaluated by calibrating the coefficient a_ρ without altering the other nuclear saturation properties. Table I provides the values of g_{iN} and $g_{\rho N}$ at n_0 . Since the non strange baryons do not couple with the ϕ meson, $g_{\phi N} = g_{\phi \Delta} = 0$.

The bare masses of baryons are considered as $m_N = 939$ MeV, $m_\Lambda = 1115.68$ MeV, $m_{\Sigma^+} = 1189.37$ MeV, $m_{\Sigma^0} = 1192.64$ MeV, $m_{\Sigma^-} = 1197.45$ MeV, $m_{\Xi^-} = 1321.71$ MeV, $m_{\Xi^0} = 1314.86$ MeV, and $m_\Delta = 1232$ MeV. The saturation property parameters, viz., n_0 , saturation energy (E_0), incompressibility (K_0), E_{sym} , L_{sym} , curvature of symmetry energy (K_{sym}), and effective nucleonic Dirac mass (m_N^*) corresponding to these parametrizations, are given in Table II.

The values of coefficient a_ρ adjusted to estimate different values of L_{sym} at n_0 for GM1 and DD-MEX parametrizations are provided in Table III, where the slope and curvature of

E_{sym} at n_0 are respectively given by

$$L_{\text{sym}}(n_0) = 3n_0 \left[\frac{\partial E_{\text{sym}}(n)}{\partial n} \right]_{n=n_0}, \quad (22)$$

$$K_{\text{sym}}(n_0) = 9n_0^2 \left[\frac{\partial^2 E_{\text{sym}}(n)}{\partial n^2} \right]_{n=n_0},$$

with the nuclear symmetry energy defined as

$$E_{\text{sym}} = \frac{1}{2} \left[\frac{\partial^2 (\varepsilon/n)}{\partial \alpha^2} \right]_{\alpha=0}, \quad (23)$$

where $\alpha = (n_n - n_p)/n$ is the asymmetry parameter.

For the hyperonic sector, the vector couplings are implemented according to SU(6) symmetry and the quark counting rule [64]. For the scalar couplings, we consider the optical potential values $U_\Lambda^N(n_0) = -30$ MeV, $U_\Sigma^N(n_0) = +30$ MeV, and $U_\Xi^N(n_0) = -14$ MeV [65,66] in symmetric nuclear matter (SNM). Recently, Ref. [67] reported an attractive optical potential for Ξ hyperons in SNM corresponding to $U_\Xi^N(n_0) \geq -20$ MeV. Table IV provides the scalar meson-hyperon coupling values at n_0 .

For the Δ -resonance sector, we consider the meson- Δ couplings as parameters. This is due to scarcity of Δ -nucleon interaction experimental data. Experimental studies [68–70] based on pion-nucleus scattering and Δ -quartet excitations have reported constraining meson- Δ -resonance couplings. Recent studies [42,46] have narrowed the Δ potential (V_Δ) in nuclear medium to be -30 MeV + $V_N \leq V_\Delta \leq V_N$ and $0 \leq R_{\sigma\Delta} - R_{\omega\Delta} \leq 0.2$ with $R_{\sigma\Delta} = g_{\sigma\Delta}/g_{\sigma N}$, $R_{\omega\Delta} = g_{\omega\Delta}/g_{\omega N}$. Several works [43,47,49,52,71] have considered the vector coupling values in the ranges $R_{\omega\Delta} \in [0.6 - 1.2]$ and $R_{\rho\Delta} \in [0.5 - 3.0]$. In the present discussion, we consider $R_{\omega\Delta} = 1.10$ and $R_{\rho\Delta} = 1.00$ in the vector coupling sector. And in the scalar-meson- Δ -resonance coupling sector, we consider $R_{\sigma\Delta} = 1.10, 1.20$.

TABLE II. The nuclear properties of the GM1 (A) and DD-MEX (B) CDF models at n_0 .

n_0 (fm ⁻³)	E_0 (MeV)	K_0 (MeV)	E_{sym} (MeV)	L_{sym} (MeV)	K_{sym} (MeV)	m_N^*/m_N
(A) 0.153	-16.30	300	32.50	93.86	17.91	0.700
(B) 0.152	-16.14	267	32.27	49.58	-71.47	0.556

TABLE III. a_ρ coefficient values for various estimations of $L_{\text{sym}}(n_0)$ and corresponding $K_{\text{sym}}(n_0)$ for GM1 and DD-MEX coupling models.

$L_{\text{sym}}(n_0)$ (MeV)	a_ρ		$K_{\text{sym}}(n_0)$ (MeV)	
	GM1	DD-MEX	GM1	DD-MEX
35	0.5893	0.8052	-127.13	-34.44
50	0.4390	0.6148	-129.67	-72.21
65	0.2888	0.4242	-105.17	-75.72
85	0.0885	0.1702	-30.43	-27.06

III. RESULTS AND DISCUSSION

In this section, we report the numerical results for purely nucleonic (N), hypernuclear (NY), and Δ -admixed hypernuclear (NY Δ) matter compositions and investigate the effects of symmetry energy on dense matter EOS. In order to do so, as mentioned in Sec. I, we implement the density-dependent modification in isovector $g_{\rho b}$ couplings within the nonlinear framework with GM1 parametrization and consider the density-dependent coupling scheme with DD-MEX parametrization. We proceed by studying the effect of variation of L_{sym} on different properties of matter and stars.

The behavior of nuclear symmetry energy with varying baryon number density is plotted in Fig. 1 for different values of L_{sym} . In density regime $n < n_0$, cases with higher values of L_{sym} yield lower values of E_{sym} while the opposite is observed in cases of higher density regimes ($n > n_0$). The experimental constraints on $E_{\text{sym}}(n)$ at subsaturation densities, shown by the shaded region in Fig. 1 allows EOSs with $L_{\text{sym}}(n_0) \geq 50$ MeV. The values of E_{sym} at n_0 are the same for all values of L_{sym} as they are constrained by the isovector coupling value at nuclear saturation. This result is consistent with that of Ref. [32] found by considering NL3 [75] parametrization. The constraint on $E_{\text{sym}}(2n_0)$ is broader and allows for almost all EOSs corresponding to $L_{\text{sym}}(n_0)$ values considered in this work.

Figure 2 displays the density-dependent nature of isovector couplings versus baryon number density for different values of L_{sym} in both coupling schemes. In subsaturation densities, it is observed that with lower L_{sym} values the isovector coupling values are larger. This behavior is opposite in suprasaturation density regimes. At the saturation density, $g_{\rho N}$ values are identical owing to Eq. (19). With higher values of L_{sym} , the variation of $g_{\rho N}$ with baryon number density is found to be more steep. The $g_{\rho N}(n)$ coupling values with lower L_{sym} approach zero at high density regimes resulting in similar corresponding $E_{\text{sym}}(n)$ values at those densities.

TABLE IV. Scalar meson-hyperon coupling constants, $R_{\sigma Y} = g_{\sigma Y}/g_{\sigma N}$ (normalized to meson-nucleon coupling) for considered parametrizations in this work.

	Λ	Σ	Ξ
GM1	0.6164	0.4033	0.3047
DD-MEX	0.6172	0.4734	0.3088

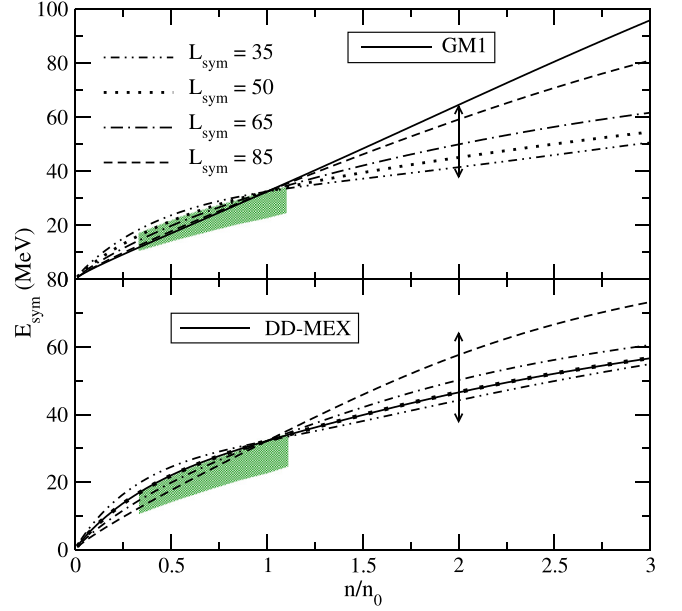


FIG. 1. Nuclear symmetry energy as a function of baryon number density (in units of n_0) for [upper panel] GM1 and [lower panel] DD-MEX coupling parametrizations. The shaded regions denote the constraints on density-dependent symmetry energy from heavy-ion collision data [72,73]. The constraint $38 \leq E_{\text{sym}}(2n_0)/\text{MeV} \leq 64$ [74] at 68% confidence level obtained via analyses of data from recent NS observables and heavy-ion collisions is denoted by the vertical error bars. The solid lines in both the panels represent the original coupling parametrizations. The other cases with adjusted values of L_{sym} at n_0 are denoted by dot-dot-dashed ($L_{\text{sym}} = 35$), dotted ($L_{\text{sym}} = 50$), dash-dotted ($L_{\text{sym}} = 65$), and dashed ($L_{\text{sym}} = 85$) curves respectively.

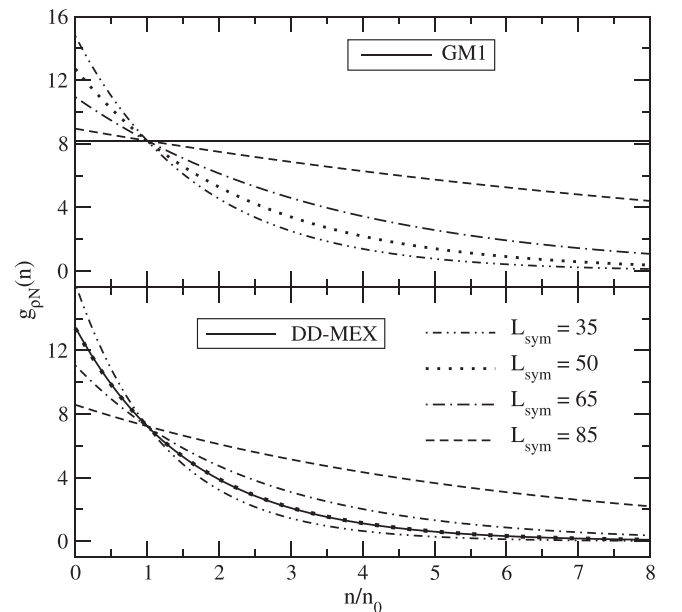


FIG. 2. Isovector coupling to nucleons as a function of baryon number density (in units of n_0) in cases of GM1 (upper panel) and DD-MEX (lower panel) parametrizations. The different curves represent the same cases as described in the caption of Fig. 1.

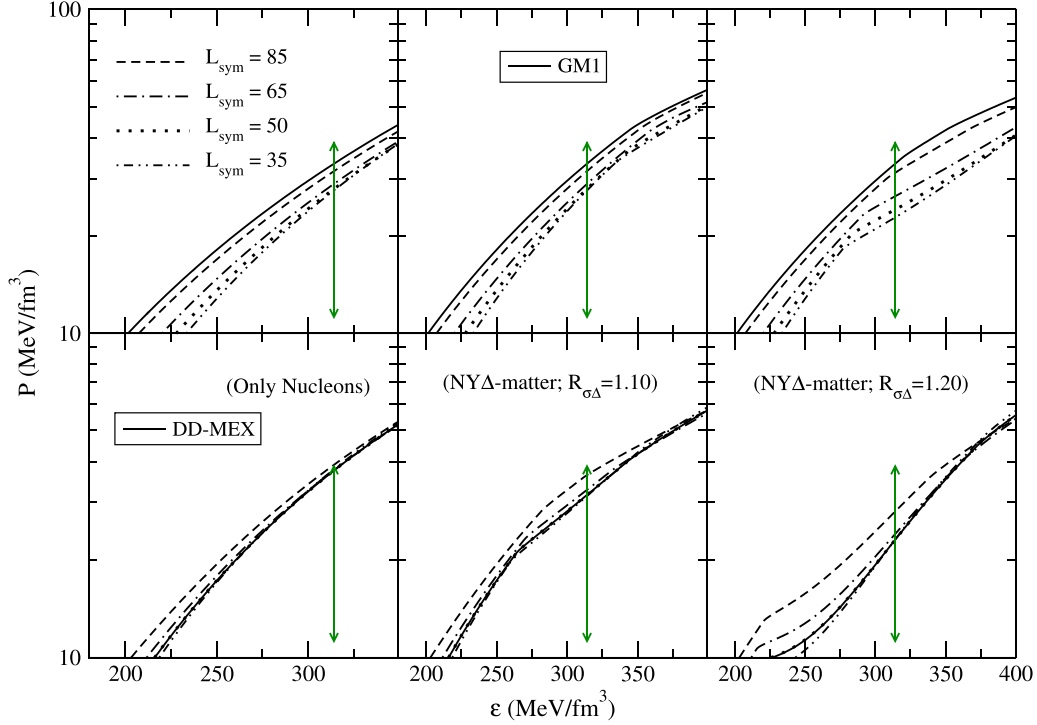


FIG. 3. Pressure variation as a function of energy density (EOS) for $T = 0$ case with matter compositions as [left panels] pure nucleonic, [middle panels] NY Δ ($R_{\sigma\Delta} = 1.10$), and [right panels] NY Δ ($R_{\sigma\Delta} = 1.20$), for different $L_{\text{sym}}(n_0)$ values in [upper panels] GM1 and [lower panels] DD-MEX parametrizations. The different curves represent the same cases as described in the caption of Fig. 1. The matter pressure constraint (vertical line) at $n \sim 2n_0$ is deduced from GW170817 [13] event data.

The EOSs for different NS matter compositions (N, NY Δ) are presented in Fig. 3 for GM1 parametrization in upper panels and for DD-MEX parametrization in lower panels. The EOSs with modified isovector couplings within the nonlinear GM1 model as well as with DD-MEX parametrization are observed to lie well within the bounds of the matter pressure constraint from GW170817 event data [13], shown by the vertical arrows in Fig. 3. This is true for all the matter composition cases. The prominent differences in EOSs are observed in low density regimes ($n \leq 0.4 \text{ fm}^{-3}$).

Tables V and VI provide the threshold densities of heavier baryons in NY and NY Δ matter with GM1 and DD-MEX coupling parametrizations respectively. It is observed that low values of L_{sym} shift the onset of hyperons to higher density regimes, while the opposite behavior is seen in case of

TABLE V. Threshold densities n_u (in units of n_0) for hyperons and Δ quartets in NY and NY Δ matter with varying $L_{\text{sym}}(n_0)$ values in GM1 parametrization.

Model	$R_{\sigma\Delta} = 0$	$R_{\sigma\Delta} = 1.10$		$R_{\sigma\Delta} = 1.20$	
	$n_u^Y(n_0)$	$n_u^Y(n_0)$	$n_u^\Delta(n_0)$	$n_u^Y(n_0)$	$n_u^\Delta(n_0)$
GM1	2.25	2.25	2.89	2.29	2.11
$L_{\text{sym}} = 35$	2.54	2.68	2.22	2.95	1.87
$L_{\text{sym}} = 50$	2.49	2.57	2.27	2.84	1.90
$L_{\text{sym}} = 65$	2.42	2.43	2.35	2.66	1.94
$L_{\text{sym}} = 85$	2.30	2.30	2.61	2.39	2.04

Δ resonances. Higher values of normalized scalar-meson- Δ couplings denote attractive Δ potentials in SNM which result in early appearance of Δ quartets in NS matter. Onset of Δ resonances delays the appearance of hyperons in NS matter.

It is observed that onset of heavier baryons softens the EOSs, marked by changes in slope, as shown in Fig. 3. Now at high matter densities, $g_{\rho b}(n)$ coupling values tend to approach zero, resulting in less contribution to EOSs from ρ -meson fields. With increase in attractive Δ potential, the onset of Δ^- shifts towards lower density regimes as marked by the kinks in Fig. 3.

The mass-radius relationships obtained by solving TOV equations for nonrotating, spherically symmetric stars corresponding to the EOSs for N, NY Δ ($R_{\sigma\Delta} = 1.10, 1.20$) matter with GM1 and DD-MEX parametrizations are displayed in different panels of Fig. 4. For the crust region, the Baym-Pethick-Sutherland (BPS) [77] EOS is implemented

TABLE VI. Similar to Table V but with DD-MEX parametrization.

Model	$R_{\sigma\Delta} = 0$	$R_{\sigma\Delta} = 1.10$		$R_{\sigma\Delta} = 1.20$	
	$n_u^Y(n_0)$	$n_u^Y(n_0)$	$n_u^\Delta(n_0)$	$n_u^Y(n_0)$	$n_u^\Delta(n_0)$
DD-MEX	2.13	2.27	1.79	2.47	1.46
$L_{\text{sym}} = 35$	2.15	2.31	1.77	2.51	1.44
$L_{\text{sym}} = 50$	2.13	2.27	1.79	2.47	1.46
$L_{\text{sym}} = 65$	2.09	2.19	1.82	2.39	1.47
$L_{\text{sym}} = 85$	2.03	2.07	1.89	2.24	1.50

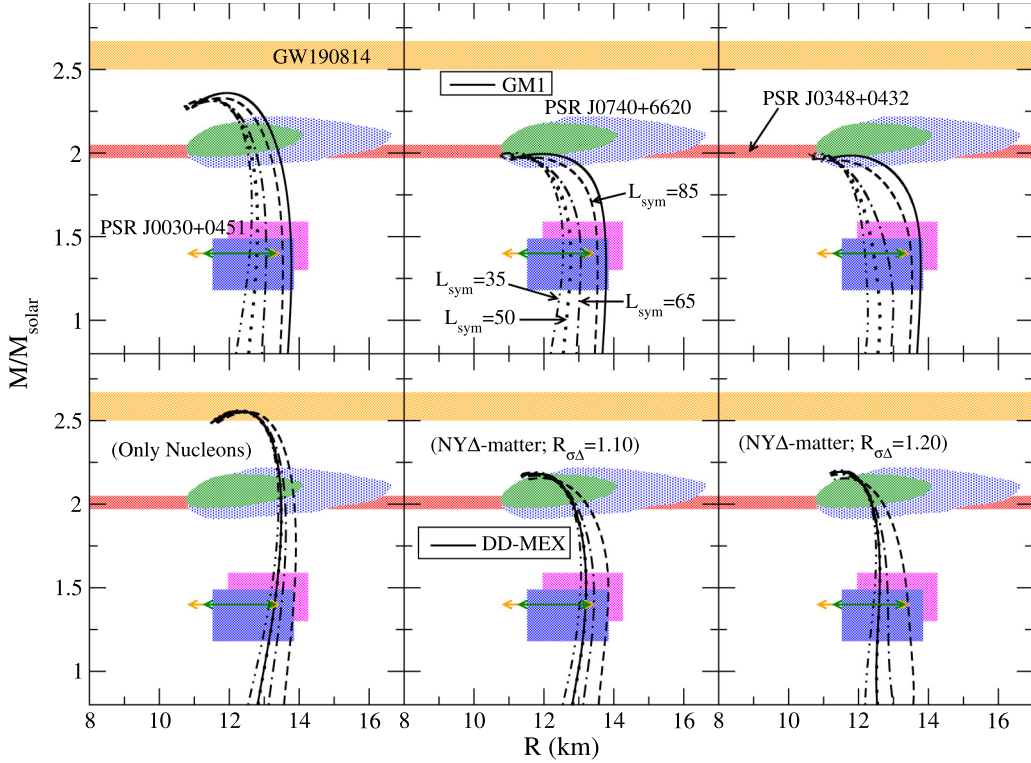


FIG. 4. Solutions of TOV equations corresponding to [left panels] pure N matter, [middle panels] NY Δ ($R_{\sigma\Delta} = 1.10$), and [right panels] NY Δ ($R_{\sigma\Delta} = 1.20$) EOSs displayed in Fig. 3, for [upper panels] GM1 and [lower panels] DD-MEX parametrizations. The different curves represent the same cases as described in the caption of Fig. 1. The astrophysical observable constraints from GW190814 [76], PSR J0740+6620 [10,11], PSR J0348+0432 [18], and PSR J0030+0451 [7,8] are represented by shaded regions. The horizontal lines represent the joint radius constraints from PSR J0030+0451 and the GW170817 event data for a typical $1.4M_{\odot}$ NS [9,20].

maintaining thermodynamic consistency with modeling the crust-core transition following Ref. [78]. It can be observed that almost all EOSs (in N and NY Δ matter compositions) fit within the limits of recent astrophysical constraints. However, the joint constraints on radius of a $1.4M_{\odot}$ NS [9,20] are satisfied by EOS models with $L_{\text{sym}} \leq 65$ MeV. Incorporation of Δ quartets further softens the EOS at lower density in addition to high density regimes, leading to NS configurations with smaller radii, as is evident from middle and right panels of Fig. 4. The nature of the secondary compact component involved in GW190814 as a NS is still not completely resolved [79,80], hence the maximum mass constraint from this candidate is not so stringent. The variation of symmetry energy slope has slight impact on maximum mass NS configurations owing to the similar values of M_{max} (refer to Table VII). The softening of EOSs due to inclusion of Δ resonances is more prominent in the density-dependent scenario. The effect of varying L_{sym} is least for pure nucleonic matter and large for NY Δ matter (with more attractive Δ potential). For DD-MEX coupling parametrization, the maximum mass NS configuration with purely nucleonic matter reaches $\sim 2.55M_{\odot}$, satisfying the mass constraint from the GW190814 event. This is consistent with the results in Ref. [81].

The particle abundances in NY Δ matter composition ($R_{\sigma\Delta} = 1.20$) with GM1 (without density-dependent $g_{\rho N}$) and with $L_{\text{sym}}(n_0) = 50$ MeV coupling parametrization

models are shown in Fig. 5. It is observed that in the case of density-dependent $g_{\rho N}(n)$ coupling (lower panel), the onset of hyperons is shifted to higher densities and early appearance of Δ resonances is favored. This results in faster decrease of lepton populations in comparison to the constant $g_{\rho N}(n_0)$ coupling case (upper panel). In the $g_{\rho N}(n_0)$ case, the Δ^- , Ξ^- , e^- , μ^- composition provides the negative charge to balance the proton charge resulting in appearance of Λ hyperons. In high density regimes, this negative particle composition leads to onset of Δ^0 and Ξ^0 baryons. In the case of $g_{\rho N}(n)$ couplings, the onset of Δ^0 baryons is due to the charge neutrality condition maintained by Δ^- , e^- with protons. Figure 6 displays the particle populations as a function of baryon number density similarly to Fig. 5 but with the DD-MEX parametrization for NY Δ matter. In this too, it is observed that with decreasing value of L_{sym} the onset of hyperons is shifted to higher densities while early onset of Δ quartets is favoured. At subsaturation densities, the charged particle abundances are enhanced with lower value of L_{sym} . In case of $L_{\text{sym}} = 49.57$ MeV (upper panel), the lepton populations are seen to decrease at a faster rate with rising matter density in comparison to the $L_{\text{sym}} = 85$ MeV (lower panel) case. This is because in the latter case Δ^- abundances fall short to maintain the charge neutrality condition, with protons causing lepton populations to remain up to higher density regimes.

In order to see the effect of varying L_{sym} on hyperons, we plot the strangeness fraction as a function of baryon number

TABLE VII. NS properties evaluated from the EOS considering various matter compositions (N, NY, NY Δ) with varying $L_{\text{sym}}(n_0)$ values with nonlinear (GM1) and density-dependent (DD-MEX) coupling schemes. The maximum gravitational mass NS and its corresponding radius are denoted by M_{max} (in units of M_{\odot}) and R (in units of km) respectively; central number density, central energy density, and central matter pressure are represented by n_c (in units of fm^{-3}), ε_c , and P_c (in units of MeV/fm^3). Matter pressures at 2 and 6 times saturation densities are denoted by $P(2n_0)$ and $P(6n_0)$ respectively. The global properties such as radius, compactness parameter, tidal Love number, and tidal deformability for a $1.4M_{\odot}$ NS are given by $R_{1.4}$ (in units of km), $C_{1.4}$, $k_{2(1.4)}$, and $\Lambda_{1.4}$ respectively.

matter composition	CDF model	M_{max} (M_{\odot})	R (km)	n_c (fm^{-3})	ε_c (MeV/fm^3)	P_c (MeV/fm^3)	$P(2n_0)$ (MeV/fm^3)	$P(6n_0)$ (MeV/fm^3)	$R_{1.4}$ (km)	$C_{1.4}$	$k_{2(1.4)}$	$\Lambda_{1.4}$
Pure nucleonic matter	GM1	2.36	11.93	0.865	1116.75	500.67	30.48	574.12	13.77	0.150	0.100	882
	$L_{\text{sym}} = 85$	2.33	11.77	0.888	1145.36	512.52	28.62	553.83	13.53	0.153	0.098	785
	NL $L_{\text{sym}} = 65$	2.31	11.51	0.917	1185.47	547.87	25.54	549.66	13.06	0.158	0.096	640
	$L_{\text{sym}} = 50$	2.32	11.45	0.919	1186.87	555.04	24.22	554.15	12.79	0.162	0.096	581
	$L_{\text{sym}} = 35$	2.33	11.42	0.916	1180.98	553.01	23.59	556.13	12.58	0.164	0.102	568
	DD-MEX	2.56	12.33	0.776	1000.40	487.24	32.26	704.96	13.29	0.156	0.106	773
	$L_{\text{sym}} = 85$	2.55	12.50	0.767	988.90	469.57	34.70	698.51	13.84	0.149	0.105	939
	DD $L_{\text{sym}} = 65$	2.55	12.36	0.777	1003.21	486.80	32.74	703.14	13.49	0.153	0.104	821
	$L_{\text{sym}} = 50$	2.56	12.33	0.776	1000.68	487.42	32.27	704.93	13.30	0.155	0.105	772
	$L_{\text{sym}} = 35$	2.56	12.31	0.773	995.26	484.09	32.31	705.36	13.14	0.157	0.108	748
Hypernuclear matter	GM1	1.99	11.97	0.926	1126.57	317.96	30.48	312.09	13.77	0.150	0.101	882
	$L_{\text{sym}} = 85$	1.98	11.72	0.964	1179.58	345.34	28.62	310.77	13.53	0.153	0.098	785
	NL $L_{\text{sym}} = 65$	1.98	11.41	1.001	1233.99	382.86	25.54	317.59	13.06	0.158	0.095	639
	$L_{\text{sym}} = 50$	2.00	11.37	0.994	1222.21	379.64	24.22	320.41	12.79	0.162	0.096	581
	$L_{\text{sym}} = 35$	2.01	11.36	0.983	1203.98	371.28	23.59	321.37	12.58	0.164	0.102	568
	DD-MEX	2.18	12.00	0.875	1082.30	362.19	32.26	395.89	13.29	0.156	0.106	777
	$L_{\text{sym}} = 85$	2.16	12.14	0.876	1085.95	357.77	34.70	390.54	13.83	0.149	0.105	937
	DD $L_{\text{sym}} = 65$	2.17	12.02	0.882	1093.24	367.13	32.74	395.07	13.49	0.153	0.104	821
	$L_{\text{sym}} = 50$	2.18	12.00	0.876	1082.86	362.48	32.27	395.88	13.30	0.155	0.105	774
	$L_{\text{sym}} = 35$	2.19	11.99	0.869	1071.27	356.43	32.31	396.04	13.14	0.157	0.108	748
Δ -admixed hypernuclear matter ($R_{\sigma\Delta} = 1.10$)	GM1	1.99	11.95	0.928	1130.21	320.17	30.48	312.53	13.77	0.150	0.101	882
	$L_{\text{sym}} = 85$	1.97	11.63	0.980	1204.54	360.38	28.62	312.22	11.63	0.153	0.098	785
	NL $L_{\text{sym}} = 65$	1.97	11.19	1.045	1302.99	428.33	25.54	324.02	13.05	0.158	0.095	637
	$L_{\text{sym}} = 50$	1.99	11.13	1.042	1297.38	429.21	24.22	328.62	12.77	0.162	0.095	570
	$L_{\text{sym}} = 35$	2.00	11.11	1.031	1278.87	420.59	23.59	330.15	12.55	0.165	0.100	551
	DD-MEX	2.18	11.75	0.911	1138.96	405.08	28.03	406.19	13.19	0.157	0.102	717
	$L_{\text{sym}} = 85$	2.16	11.92	0.909	1138.40	395.67	33.15	398.31	13.83	0.149	0.104	935
	DD $L_{\text{sym}} = 65$	2.17	11.76	0.918	1152.14	411.28	29.43	405.19	13.43	0.154	0.102	788
	$L_{\text{sym}} = 50$	2.18	11.75	0.911	1139.52	405.38	28.06	406.18	13.20	0.157	0.102	720
	$L_{\text{sym}} = 35$	2.19	11.74	0.904	1127.36	398.93	27.51	406.38	13.02	0.159	0.104	686
Δ -admixed hypernuclear matter ($R_{\sigma\Delta} = 1.20$)	GM1	1.99	11.78	0.962	1179.86	345.22	30.48	313.94	13.77	0.150	0.101	881
	$L_{\text{sym}} = 85$	1.96	11.34	1.037	1290.93	410.47	28.62	316.04	13.50	0.153	0.097	773
	NL $L_{\text{sym}} = 65$	1.97	10.87	1.102	1392.46	488.48	24.65	332.45	12.82	0.161	0.089	541
	$L_{\text{sym}} = 50$	1.98	10.82	1.094	1377.87	485.28	22.32	338.37	12.43	0.166	0.086	449
	$L_{\text{sym}} = 35$	2.00	10.81	1.083	1358.24	476.19	20.88	340.33	12.18	0.169	0.083	395
	DD-MEX	2.19	11.48	0.938	1177.66	439.80	18.67	416.19	12.59	0.164	0.090	505
	$L_{\text{sym}} = 85$	2.15	11.62	0.945	1193.37	436.81	24.49	405.46	13.41	0.154	0.094	720
	DD $L_{\text{sym}} = 65$	2.18	11.48	0.947	1194.49	447.69	20.08	414.88	12.84	0.161	0.089	565
	$L_{\text{sym}} = 50$	2.19	11.48	0.938	1177.94	439.93	18.69	416.17	12.59	0.164	0.090	506
	$L_{\text{sym}} = 35$	2.20	11.47	0.930	1165.22	433.33	18.30	416.43	12.43	0.166	0.093	487

density in Fig. 7, defined as [82]

$$f_s = \frac{1}{3} \frac{\sum_Y |s_Y| n_Y}{n}, \quad (24)$$

where s_Y , n_Y denote the strangeness and number density of Y th hyperon respectively. It is seen that f_s is sensitive to varying L_{sym} and decreases with lowering L_{sym} values. The

shifting of hyperon threshold densities to higher densities with lower values of L_{sym} (as seen in Figs. 5 and 6) is also evident from Fig. 7. The similar strangeness fraction for $L_{\text{sym}} = 65, 50, 35$ MeV cases at high densities relates with the almost similar values (approaching zero) of $g_{\rho N}(n)$ (refer to Fig. 2). In both the coupling parametrization cases, similar f_s values at high density regimes relate to the almost vanishing values of ρ -meson coupling. The delaying appearance of hyperons

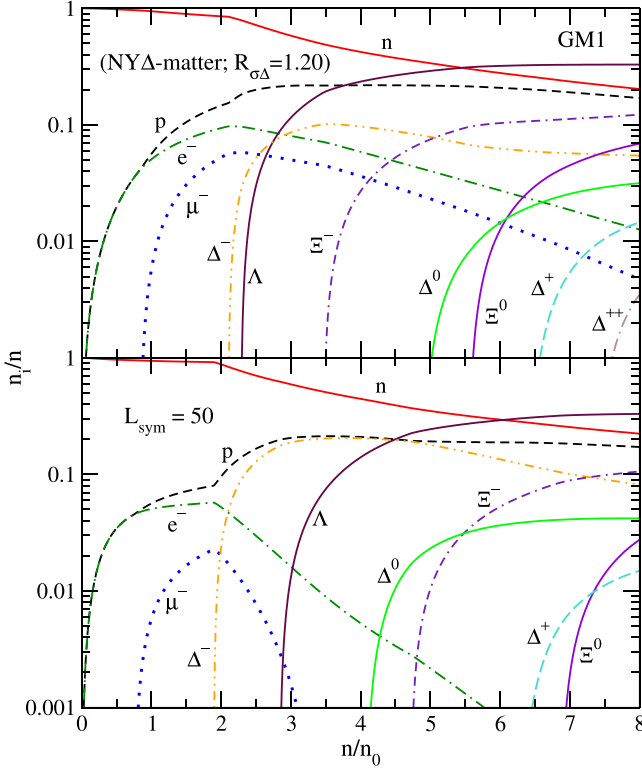


FIG. 5. Particle populations n_i (in units of n) as a function of baryon number density for NY Δ matter ($R_{\sigma\Delta} = 1.20$) with [upper panel] $L_{\text{sym}}(n_0) = 93.86$ MeV (original) and [lower panel] $L_{\text{sym}}(n_0) = 50$ MeV cases within the nonlinear coupling (GM1) parametrization.

into NS matter with onset of Δ quartets is also apparent in Fig. 7.

Due to the utmost dependence of matter pressure explicitly over energy density in NS matter, it is noteworthy that the EOSs follow the causality condition (i.e., adiabatic speed velocity v_s to be subluminal) given by $v_s < c$. Fig. 8 displays the adiabatic speed of sound as a function of energy density for different matter compositions with variation in L_{sym} values within nonlinear and density-dependent CDF models. It is observed that the EOSs considered in this work satisfy the causality condition. The effect of L_{sym} is more prominent in the lower density regimes. This can be attributed to the diverse $g_{\rho N}$ coupling values at lower densities. Lower values of L_{sym} result in reduced v_s at lower matter densities. Kinks in the lower panels denote onset of heavier baryons in NS matter.

Now we move to examine the effect of L_{sym} on star properties. The properties of NSs for variation of L_{sym} along with matter properties with different EOSs considered in this work are displayed in Table VII. L_{sym} has practically no effect on the maximum mass of the star family. However, L_{sym} variation has a commendable impact on the radius of NS configurations. This feature is already clear from Fig. 4. We have tabulated the comparative values of radius for typical $1.4M_{\odot}$ mass NSs ($R_{1.4}$). With increasing value of L_{sym} the $R_{1.4}$ increases. Consequently, the compactness $C_{1.4}$ decreases. Similar impact is also observed in case of tidal deformability

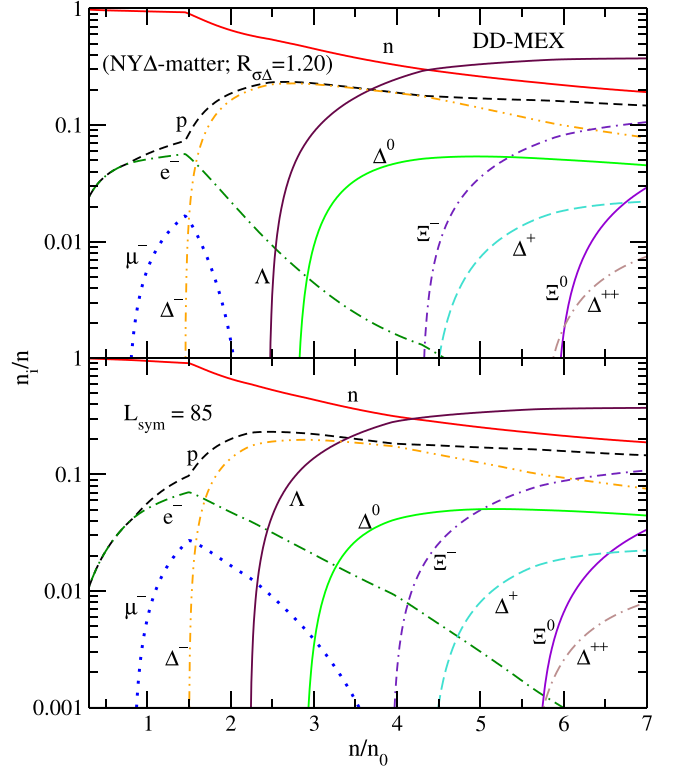


FIG. 6. Similar to Fig. 5 but with [upper panel] $L_{\text{sym}}(n_0) = 49.57$ MeV (original) and [lower panel] $L_{\text{sym}}(n_0) = 85$ MeV cases within the density-dependent coupling (DD-MEX) parametrization.

$\Lambda_{1.4}$: with increase of L_{sym} softness decreases. A recent study [83] based on the joint analysis GW170817 and GW190425 events data reported a radius bound of $10.94 \leq R_{1.4}/\text{km} \leq 12.61$ at 90% confidence level. From the EOSs considered in this work, it can be inferred that, to satisfy the said $R_{1.4}$ range, the conditions of Δ -resonances onset into NS matter composition and $L_{\text{sym}}(n_0) \leq 50$ MeV are favorable. Following the $69 \leq L_{\text{sym}}(n_0)/\text{MeV} \leq 143$ range deduced from recent PREX-2 data, it is to be noted that the DD-MEX parametrization satisfies the $\Lambda_{1.4}$ upper bound (GW170817 event) for $L_{\text{sym}}(n_0) \leq 85$ with $R_{\sigma\Delta} = 1.20$.

The variations of compactness parameter and tidal deformability of a $1.4M_{\odot}$ NS with L_{sym} considering various matter compositions are shown in Fig. 9. The softness decreases in both parametrizations following a similar trend of convergence towards higher L_{sym} values. This relates to the fact that decreasing L_{sym} shifts the onset of Δ quartets to lower density regimes thus increasing compactness and decreasing tidal deformability. The quadratic fit of the compactness parameter and tidal deformability as a function of L_{sym} for different matter compositions with GM1 and DD-MEX parametrizations is given by

$$C_{1.4} \quad \text{or} \quad \Lambda_{1.4} = a L_{\text{sym}}^2 + b L_{\text{sym}} + c, \quad (25)$$

where the coefficient a , b , and c values are provided in Table VIII.

Figure 10 shows the variation of dimensionless tidal deformability with NS mass corresponding to different values of

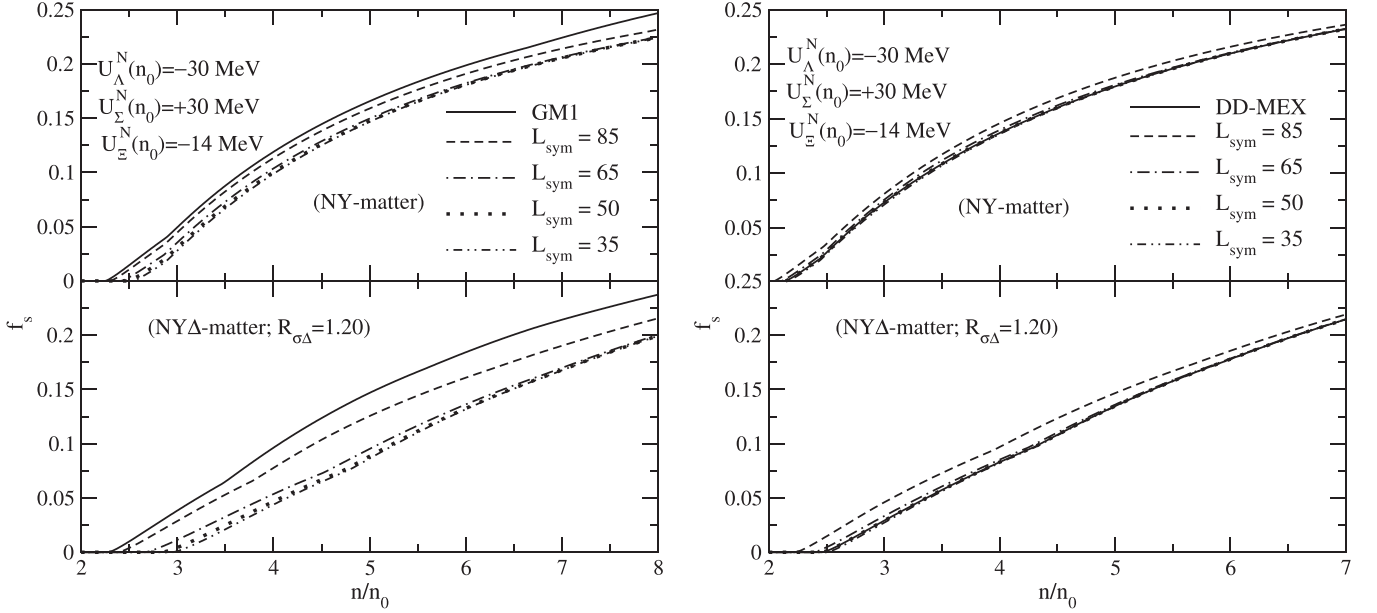


FIG. 7. Strangeness fraction, f_s as a function of baryon number density for matter composition as [upper panels] NY and [lower panels] NY Δ ($R_{\sigma\Delta} = 1.20$) with varying L_{sym} for [left panels] GM1 and [right panels] DD-MEX parametrizations. The different curves represent the same cases as described in the caption of Fig. 1.

the density-dependent L_{sym} parameter. As already mentioned, we observe that with higher values of L_{sym} the tidal deforma-

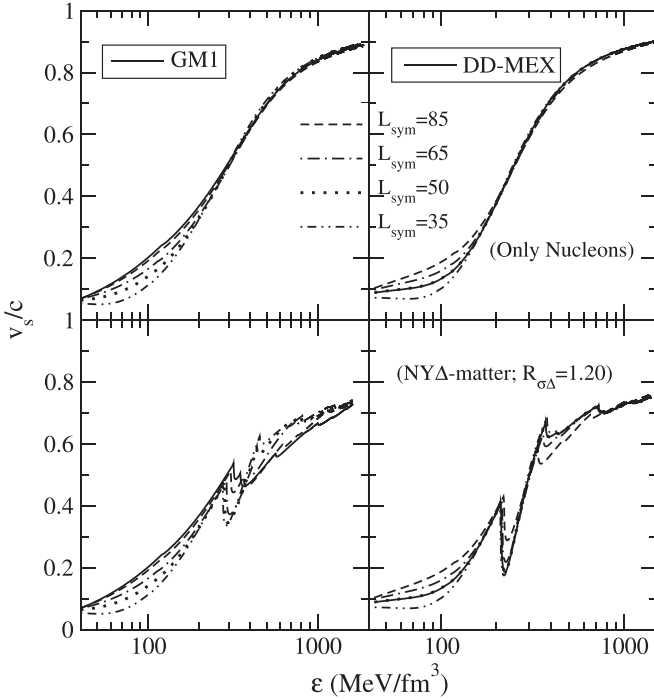


FIG. 8. Adiabatic sound velocity (in units of c) as a function of energy density for [upper panels] pure nucleonic and [lower panels] Δ -admixed hypernuclear matter ($R_{\sigma\Delta} = 1.20$), with [left panels] nonlinear (GM1) and [right panels] density-dependent (DD-MEX) coupling models. The different curves represent the same cases as described in the caption of Fig. 1.

bility parameter value increases as the matter stiffens. The effects of L_{sym} are significant only in the case of lower mass stars; for massive stars, these effects are inconsequential. In addition, the inclusion of heavier nonstrange baryons softens the EOS at lower density regimes consequently decreasing Λ or assembling NS matter to be more compact. This agrees with the results from Refs. [48,71].

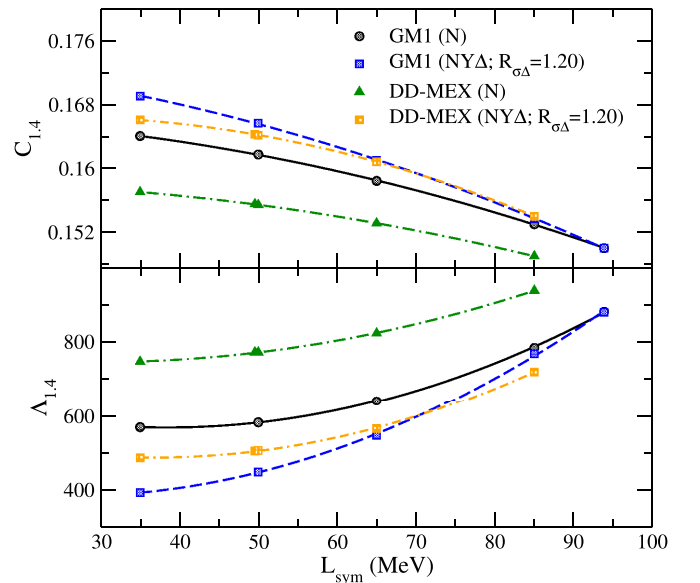


FIG. 9. Upper panel: Compactness parameter. Lower panel: Tidal deformability as a function of L_{sym} considering matter composition to be pure N, NY Δ ($R_{\sigma\Delta} = 1.20$) with nonlinear (GM1) and density-dependent (DD-MEX) coupling models. The different curves denote the EOS models as labeled.

TABLE VIII. Coefficient values of the quadratic fits in Eq. (25). The coefficient of determination $\mathcal{R}^2 \sim 0.999$ for all the fits considered in this work.

CDF Model		a	b	c
$C_{1.4}$	GM1 (N)	-1.83×10^{-6}	-2.10×10^{-6}	0.1663
	GM1 (NY Δ)	-2.01×10^{-6}	-6.51×10^{-5}	0.1738
	DD-MEX (N)	-1.53×10^{-6}	2.38×10^{-5}	0.1581
	DD-MEX (NY Δ)	-3.31×10^{-6}	0.0002	0.1646
$\Lambda_{1.4}$	GM1 (N)	0.1023	-7.884	719.10
	GM1 (NY Δ)	0.1082	-5.617	458.70
	DD-MEX (N)	0.0623	-3.676	800.80
	DD-MEX (NY Δ)	0.0998	-7.339	622.40

IV. SUMMARY AND CONCLUSIONS

In this work, we discuss the density-dependent symmetry energy effects on dense matter EOSs with different matter compositions, viz., pure nucleonic, hypernuclear, and Δ -admixed hypernuclear, within the CDF theory framework. We consider different values of symmetry energy slope L_{sym} to introduce variation of symmetry energy with density. The L_{sym} value at saturation is taken to be within the range of 35–85 MeV. The NS configurations evaluated from the EOSs considered in this work within this range of L_{sym} satisfy the recent astrophysical observable constraints obtained from

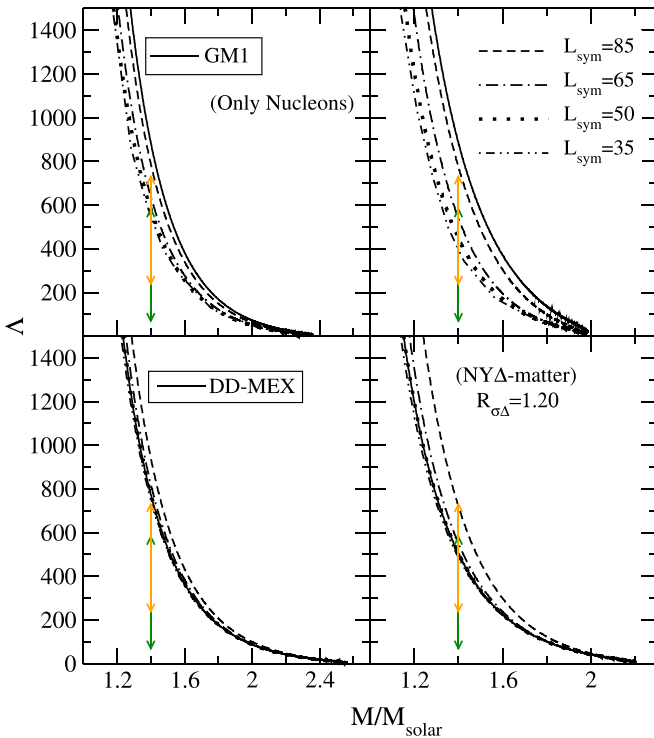


FIG. 10. Tidal deformability as a function of NS mass for [left panels] pure nucleonic and [right panels] NY Δ ($R_{\sigma\Delta} = 1.20$) matter, with varying L_{sym} values in [upper panels] GM1 and [lower panels] DD-MEX parametrizations. The different curves represent the same cases as described in the caption of Fig. 1. The vertical lines denote the bounds on $\Lambda_{1.4}$ deduced in Refs. [13,20].

NICER (PSR J0030+0451 [7,8], PSR J0740+6620 [10,11]) and GW [12,15] observations.

We find that, with smaller values of L_{sym} , the EOS is evaluated to be softer around density range of $(1-2)n_0$. This is because of the corresponding lower values of E_{sym} in the said density regimes. This results in smaller radii alongside, making the matter tidally less deformable for intermediate mass NSs, viz., $1.4M_{\odot}$. Although the range of L_{sym} considered in this work is consistent with the astrophysical observations, the lower values of L_{sym} are more favorable for the radius observations from NICER [7,8,10,11] as well as estimate of tidal deformability from GW observations. In the high density regimes, the EOS is similar for all L_{sym} values. This attributes to the vanishing ρ meson fields due to small (approaching zero) $g_{\rho N}$ coupling values.

Different values of L_{sym} also have substantial effect on the appearance of exotic components of matter. The lower values of L_{sym} shift the threshold density for appearance of hyperons to the higher side and favor early appearance of Δ -quartet particles. The early appearance of Δ particles is also one of the causes for higher threshold density for the appearance of hyperons with lower values of L_{sym} . The early appearance of Δ particles for lower values of L_{sym} makes the EOS softer in the lower density, attributed to the smaller radius for stars having mass $\sim 1.4 M_{\odot}$. Consequently, the compactness of the stars increases and the deformability decreases with the decreasing values of L_{sym} . The different values of L_{sym} do not practically affect the maximum mass of the NS family as, in the higher density regime, the effect of different values of L_{sym} on the EOS is negligible. This agrees with the results from Refs. [82,84]. As for higher values of L_{sym} , the EOSs do not differ much, and the values of compactness and tidal deformability merge at higher values of L_{sym} . Hence the possibility of exotic matter appearance with lower values of L_{sym} is most favorable from all astrophysical observations.

However, the recent update from nuclear physics sector (PREX-2) suggests higher values of $L_{\text{sym}}(n_0)$, which is in tension with the astrophysical observables, viz., tidal deformability and radius of a canonical $1.4M_{\odot}$ NS. Considering the viability of inclusion of nonrange Δ baryons into the NS dense matter EOS is seen to be a reasonable option. Moreover, different choices of coupling models and parametrizations might or might not provide a feasible solution to this tension and so may have to be recalibrated. Further analysis regarding this aspect is beyond the scope of this work and will be discussed in future studies.

The particle population of protons in β -equilibrated matter largely depends on the variation of nuclear symmetry energy with density. This in turn influences the threshold densities of nucleonic direct Urca processes consequently in cooling processes. Several studies [38,71,78,85] have been done to understand the effects of L_{sym} on this aspect. Such analysis with non-nucleonic matter composition following the recent update in isospin asymmetry parameter and L_{sym} range will also be addressed in future works.

ACKNOWLEDGMENTS

The authors thank the anonymous referee for constructive comments which enhanced the quality of the manuscript.

- [1] N. K. Glendenning, *Compact Stars*, 2nd ed. (Springer, New York, 2007).
- [2] F. Weber, *Pulsars as Astrophysical Laboratories for Nuclear and Particle Physics*, Series in High Energy Physics, Cosmology and Gravitation (CRC, Boca Raton, FL, 2017).
- [3] C. Ducoin, J. Margueron, and C. Providência, *Europhys. Lett.* **91**, 32001 (2010).
- [4] J. M. Lattimer and M. Prakash, *Phys. Rep.* **621**, 127 (2016).
- [5] M. Centelles, X. Roca-Maza, X. Viñas, and M. Warda, *Phys. Rev. Lett.* **102**, 122502 (2009).
- [6] F. J. Fattoyev, J. Piekarewicz, and C. J. Horowitz, *Phys. Rev. Lett.* **120**, 172702 (2018).
- [7] M. C. Miller, F. K. Lamb, A. J. Dittmann, S. Bogdanov, Z. Arzoumanian, K. C. Gendreau, S. Guillot, A. K. Harding, W. C. G. Ho, J. M. Lattimer, R. M. Ludlam, S. Mahmoodifar, S. M. Morsink, P. S. Ray, T. E. Strohmayer, K. S. Wood, T. Enoto, R. Foster, T. Okajima, G. Prigozhin *et al.*, *Astrophys. J. Lett.* **887**, L24 (2019).
- [8] T. E. Riley, A. L. Watts, S. Bogdanov, P. S. Ray, R. M. Ludlam, S. Guillot, Z. Arzoumanian, C. L. Baker, A. V. Bilous, D. Chakrabarty, K. C. Gendreau, A. K. Harding, W. C. G. Ho, J. M. Lattimer, S. M. Morsink, and T. E. Strohmayer, *Astrophys. J. Lett.* **887**, L21 (2019).
- [9] P. Landry, R. Essick, and K. Chatziioannou, *Phys. Rev. D* **101**, 123007 (2020).
- [10] T. E. Riley, A. L. Watts, P. S. Ray, S. Bogdanov, S. Guillot, S. M. Morsink, A. V. Bilous, Z. Arzoumanian, D. Choudhury, J. S. Deneva, K. C. Gendreau, A. K. Harding, W. C. G. Ho, J. M. Lattimer, M. Loewenstein, R. M. Ludlam, C. B. Markwardt, T. Okajima, C. Prescod-Weinstein, R. A. Remillard *et al.*, *Astrophys. J. Lett.* **918**, L27 (2021).
- [11] M. C. Miller, F. K. Lamb, A. J. Dittmann, S. Bogdanov, Z. Arzoumanian, K. C. Gendreau, S. Guillot, W. C. G. Ho, J. M. Lattimer, M. Loewenstein, S. M. Morsink, P. S. Ray, M. T. Wolff, C. L. Baker, T. Cazeau, S. Manthripragada, C. B. Markwardt, T. Okajima, S. Pollard, I. Cognard *et al.*, *Astrophys. J. Lett.* **918**, L28 (2021).
- [12] B. P. Abbott, R. Abbott, T. D. Abbott, F. Acernese, K. Ackley *et al.* (LIGO Scientific Collaboration and Virgo Collaboration), *Phys. Rev. Lett.* **119**, 161101 (2017).
- [13] B. P. Abbott, R. Abbott, T. D. Abbott, F. Acernese, K. Ackley *et al.* (The LIGO Scientific Collaboration and the Virgo Collaboration), *Phys. Rev. Lett.* **121**, 161101 (2018).
- [14] B. P. Abbott, R. Abbott, T. D. Abbott *et al.* (LIGO Scientific Collaboration and Virgo Collaboration), *Phys. Rev. X* **9**, 011001 (2019).
- [15] B. P. Abbott, R. Abbott, T. D. Abbott, S. Abraham, F. Acernese, K. Ackley, C. Adams, R. X. Adhikari, V. B. Adya, C. Affeldt *et al.*, *Astrophys. J. Lett.* **892**, L3 (2020).
- [16] P. B. Demorest, T. Pennucci, S. M. Ransom, M. S. E. Roberts, and J. W. T. Hessels, *Nature (London)* **467**, 1081 (2010).
- [17] Z. Arzoumanian *et al.* (NANOGrav Collaboration), *Astrophys. J. Suppl. Series* **235**, 37 (2018).
- [18] J. Antoniadis, P. C. C. Freire, N. Wex, T. M. Tauris, R. S. Lynch, M. H. van Kerkwijk, M. Kramer, C. Bassa, V. S. Dhillon, T. Driebe, J. W. T. Hessels, V. M. Kaspi, V. I. Kondratiev, N. Langer, T. R. Marsh, M. A. McLaughlin, T. T. Pennucci, S. M. Ransom, I. H. Stairs, J. van Leeuwen *et al.*, *Science* **340**, 448 (2013).
- [19] E. Fonseca, H. T. Cromartie, T. T. Pennucci, P. S. Ray, A. Y. Kirichenko, S. M. Ransom, P. B. Demorest, I. H. Stairs, Z. Arzoumanian, L. Guillemot, A. Parthasarathy, M. Kerr, I. Cognard, P. T. Baker, H. Blumer, P. R. Brook, M. DeCesar, T. Dolch, F. A. Dong, E. C. Ferrara *et al.*, *Astrophys. J. Lett.* **915**, L12 (2021).
- [20] J.-L. Jiang, S.-P. Tang, Y.-Z. Wang, Y.-Z. Fan, and D.-M. Wei, *Astrophys. J.* **892**, 55 (2020).
- [21] J. M. Lattimer and A. W. Steiner, *Eur. Phys. J. A* **50**, 40 (2014).
- [22] X. Roca-Maza, X. Viñas, M. Centelles, B. K. Agrawal, G. Colò, N. Paar, J. Piekarewicz, and D. Vretenar, *Phys. Rev. C* **92**, 064304 (2015).
- [23] I. Tews, J. M. Lattimer, A. Ohnishi, and E. E. Kolomeitsev, *Astrophys. J.* **848**, 105 (2017).
- [24] D. Adhikari, H. Albatineh, D. Androic *et al.* (PREX Collaboration), *Phys. Rev. Lett.* **126**, 172502 (2021).
- [25] B. T. Reed, F. J. Fattoyev, C. J. Horowitz, and J. Piekarewicz, *Phys. Rev. Lett.* **126**, 172503 (2021).
- [26] M. Oertel, M. Hempel, T. Klähn, and S. Typel, *Rev. Mod. Phys.* **89**, 015007 (2017).
- [27] W. M. Spinella, A systematic investigation of exotic matter in neutron stars, Ph.D. thesis, The Claremont Graduate University, 2017 (unpublished).
- [28] N. K. Glendenning and S. A. Moszkowski, *Phys. Rev. Lett.* **67**, 2414 (1991).
- [29] A. Taninah, S. Agbemava, A. Afanasjev, and P. Ring, *Phys. Lett. B* **800**, 135065 (2020).
- [30] F. Ji, J. Hu, S. Bao, and H. Shen, *Phys. Rev. C* **100**, 045801 (2019).
- [31] J. Hu, S. Bao, Y. Zhang, K. Nakazato, K. Sumiyoshi, and H. Shen, *Prog. Theor. Exp. Phys.* **2020**, 043D01 (2020).
- [32] X. Wu, S. Bao, H. Shen, and R. Xu, *Phys. Rev. C* **104**, 015802 (2021).
- [33] S. Weissenborn, D. Chatterjee, and J. Schaffner-Bielich, *Nucl. Phys. A* **881**, 62 (2012).
- [34] L. Bonanno and A. Sedrakian, *Astron. Astrophys.* **539**, A16 (2012).
- [35] G. Colucci and A. Sedrakian, *Phys. Rev. C* **87**, 055806 (2013).
- [36] M. Oertel, C. Providência, F. Gulminelli, and A. R. Raduta, *J. Phys. G* **42**, 075202 (2015).
- [37] L. Tolos, M. Centelles, and A. Ramos, *Publ. Astron. Soc. Aust.* **34**, e065 (2017).
- [38] A. R. Raduta, A. Sedrakian, and F. Weber, *Mon. Not. R. Astron. Soc.* **475**, 4347 (2018).
- [39] J. J. Li, W. H. Long, and A. Sedrakian, *Eur. Phys. J. A* **54**, 133 (2018).
- [40] L. L. Lopes and D. P. Menezes, *Nucl. Phys. A* **1009**, 122171 (2021).
- [41] L. L. Lopes, *Commun. Theor. Phys.* **74**, 015302 (2022).
- [42] A. Drago, A. Lavagno, G. Pagliara, and D. Pigato, *Phys. Rev. C* **90**, 065809 (2014).
- [43] B.-J. Cai, F. J. Fattoyev, B.-A. Li, and W. G. Newton, *Phys. Rev. C* **92**, 015802 (2015).
- [44] Z.-Y. Zhu, A. Li, J.-N. Hu, and H. Sagawa, *Phys. Rev. C* **94**, 045803 (2016).
- [45] H. S. Sahoo, G. Mitra, R. Mishra, P. K. Panda, and B.-A. Li, *Phys. Rev. C* **98**, 045801 (2018).
- [46] E. Kolomeitsev, K. Maslov, and D. Voskresensky, *Nucl. Phys. A* **961**, 106 (2017).
- [47] J. J. Li, A. Sedrakian, and F. Weber, *Phys. Lett. B* **783**, 234 (2018).
- [48] J. J. Li and A. Sedrakian, *Astrophys. J. Lett.* **874**, L22 (2019).

- [49] P. Ribes, A. Ramos, L. Tolos, C. Gonzalez-Boquera, and M. Centelles, *Astrophys. J.* **883**, 168 (2019).
- [50] J. J. Li, A. Sedrakian, and M. Alford, *Phys. Rev. D* **101**, 063022 (2020).
- [51] V. B. Thapa, M. Sinha, J. J. Li, and A. Sedrakian, *Particles* **3**, 660 (2020).
- [52] V. B. Thapa, A. Kumar, and M. Sinha, *Mon. Not. R. Astron. Soc.* **507**, 2991 (2021).
- [53] M. Mannarelli, *Particles* **2**, 411 (2019).
- [54] P. Haensel and M. Proszynski, *Astrophys. J.* **258**, 306 (1982).
- [55] N. K. Glendenning and J. Schaffner-Bielich, *Phys. Rev. C* **60**, 025803 (1999).
- [56] S. Banik and D. Bandyopadhyay, *Phys. Rev. C* **63**, 035802 (2001).
- [57] M. Prakash, I. Bombaci, M. Prakash, P. J. Ellis, J. M. Lattimer, and R. Knorren, *Phys. Rep.* **280**, 1 (1997).
- [58] T. Malik, S. Banik, and D. Bandyopadhyay, *Eur. Phys. J. Spec. Top.* **230**, 561 (2021).
- [59] V. B. Thapa and M. Sinha, *Phys. Rev. D* **102**, 123007 (2020).
- [60] V. B. Thapa, M. Sinha, J. J. Li, and A. Sedrakian, *Phys. Rev. D* **103**, 063004 (2021).
- [61] T. Hinderer, *Astrophys. J.* **677**, 1216 (2008).
- [62] T. Binington and E. Poisson, *Phys. Rev. D* **80**, 084018 (2009).
- [63] M. Favata, *Phys. Rev. Lett.* **112**, 101101 (2014).
- [64] J. Schaffner, C. Dover, A. Gal, C. Greiner, D. Millener, and H. Stocker, *Ann. Phys. (NY)* **235**, 35 (1994).
- [65] R. O. Gomes, V. Dexheimer, S. Schramm, and C. A. Z. Vasconcellos, *Astrophys. J.* **808**, 8 (2015).
- [66] A. Gal, E. V. Hungerford, and D. J. Millener, *Rev. Mod. Phys.* **88**, 035004 (2016).
- [67] E. Friedman and A. Gal, *Phys. Lett. B* **820**, 136555 (2021).
- [68] J. Koch and N. Ohtsuka, *Nucl. Phys. A* **435**, 765 (1985).
- [69] K. Wehrberger, C. Bedau, and F. Beck, *Nucl. Phys. A* **504**, 797 (1989).
- [70] S. X. Nakamura, T. Sato, T.-S. H. Lee, B. Szczerbinska, and K. Kubodera, *Phys. Rev. C* **81**, 035502 (2010).
- [71] A. R. Raduta, *Phys. Lett. B* **814**, 136070 (2021).
- [72] M. B. Tsang, Y. Zhang, P. Danielewicz, M. Famiano, Z. Li, W. G. Lynch, and A. W. Steiner, *Phys. Rev. Lett.* **102**, 122701 (2009).
- [73] M. Tsang, Z. Chajecki, D. Coupland, P. Danielewicz, F. Famiano, R. Hodges, M. Kilburn, F. Lu, W. Lynch, J. Winkelbauer, M. Youngs, and Y. Zhang, *Prog. Part. Nucl. Phys.* **66**, 400 (2011).
- [74] B.-A. Li, B.-J. Cai, W.-J. Xie, and N.-B. Zhang, *Universe* **7**, 182 (2021).
- [75] G. A. Lalazissis, J. König, and P. Ring, *Phys. Rev. C* **55**, 540 (1997).
- [76] R. Abbott, T. D. Abbott, S. Abraham, F. Acernese, K. Ackley, C. Adams, R. X. Adhikari, V. B. Adya, C. Affeldt, M. Agathos *et al.*, *Astrophys. J. Lett.* **896**, L44 (2020).
- [77] G. Baym, C. Pethick, and P. Sutherland, *Astrophys. J.* **170**, 299 (1971).
- [78] M. Fortin, C. Providência, A. R. Raduta, F. Gulminelli, J. L. Zdunik, P. Haensel, and M. Bejger, *Phys. Rev. C* **94**, 035804 (2016).
- [79] A. Sedrakian, F. Weber, and J. J. Li, *Phys. Rev. D* **102**, 041301(R) (2020).
- [80] J. J. Li, A. Sedrakian, and F. Weber, *Phys. Lett. B* **810**, 135812 (2020).
- [81] I. A. Rather, U. Rahaman, M. Imran, H. C. Das, A. A. Usmani, and S. K. Patra, *Phys. Rev. C* **103**, 055814 (2021).
- [82] R. Cavagnoli, D. P. Menezes, and C. Providência, *Phys. Rev. C* **84**, 065810 (2011).
- [83] T. Dietrich, M. W. Coughlin, P. T. H. Pang, M. Bulla, J. Heinzl, L. Issa, I. Tews, and S. Antier, *Science* **370**, 1450 (2020).
- [84] C. Providência and A. Rabhi, *Phys. Rev. C* **87**, 055801 (2013).
- [85] A. W. Steiner, *Phys. Rev. C* **74**, 045808 (2006).